*International Journal of Microwave and Wireless Technologies*

**cambridge.org/mrf**

# Design and analysis of a circularly polarized Nabla-slotted waveguide antenna for reflector application

R. R. Sorna Kumar and Indumathi Ganesan

Electronics and Communication Engineering, Mepco Schlenk Engineering College, Sivakasi, India

## Research Paper

**Cite this article:** Sorna Kumar RR, Ganesan I (2025) Design and analysis of a circularly polarized Nabla-slotted waveguide antenna for reflector application. *International Journal of Microwave and Wireless Technologies* **17**(10), 1883–1894. https://doi.org/10.1017/S1759078725102742

Received: 25 August 2025
Revised: 4 December 2025
Accepted: 10 December 2025

**Keywords:**
circular polarization; Ku-band; Nabla slot (NS); offset parabolic reflector; waveguide antenna

**Corresponding author:** R. R. Sorna Kumar; Email: sornakumarrr@mepcoeng.ac.in

Ganesan Indumathi is a contributing author.

**Abstract**

A novel compact Ku-band waveguide antenna is proposed that offers left-hand circular polarization (LHCP). The proposed design has Nabla slot on aperture of circular waveguide to attain LHCP. Side fed design of the proposed antenna eliminates the need for rectangular to circular waveguide transition. The antenna has the reflection coefficient ($S_{11}$) below −10 dB from 12 to 15.2 GHz, corresponds to the impedance bandwidth of 23.5% and axial ratio (AR) below 3 dB from 13.2 to 15.2 GHz, attained circular polarization bandwidth as 14%. Measurement results indicate that the proposed antenna achieves a 12 dB half beamwidth of around 65° across the 13.4–15.2 GHz frequency band, resulting in an attained pattern bandwidth (stable radiation pattern range) of 12.5%. This performance fulfills the illumination requirements for an offset parabolic reflector with an $f/R_D$ ratio of 0.25.

## Introduction

In space communication, polarization mismatch and signal attenuation pose significant challenges. Antennas are designed for specific polarization states. Polarization mismatch, leading to signal loss, occurs when antenna misalignment or differing polarization states exist between transmitting and receiving antennas. Maintaining precise antenna alignment, crucial to prevent this mismatch, is particularly challenging in space due to dynamic satellite movement and environmental factors. Similarly, in order to maintain reliable off-body communication links (positioning of the antenna over the body), wearable multiple-input–multiple-output antenna systems must ensure proper antenna alignment. Circularly polarized (CP) antennas offer a promising mitigation strategy. CP antennas exhibit insensitivity to antenna misalignment in up/downlink, inter-satellite communication scenarios and off-body communication. Faraday rotation, an ionospheric effect, rotates the polarization plane of radio signals, causing substantial signal loss (≥3 dB) for linear polarization, which degrades ground-to-Satellite data transmission. CP antennas counteract this effect, ensuring signal integrity [1, 2]. The integration of a CP feed source with a reflector antenna offers a high-gain solution for space-to ground satellite communications [3, 4]. Most feeds are waveguide-based due to their simple geometry and high power handling capacity. Circular waveguides are particularly preferred for efficient reflector illumination with low cross-polarization. A CP waveguide antenna usually consist of a polarizer which converts linearly polarized (LP) input waves into CP waves. Conventional waveguide polarizers typically employ miniature structures, such as irises and ridges [5–9], within the waveguide cavity. These components demand stringent manufacturing tolerances for high-frequency CP applications. Dielectric slab based polarizer [10] has wide operating bandwidth but not suitable for high vibrating environment. To circumvent these challenges, antipodal tapered slot antenna (ATSA) and constant width slot antenna (CWSA) was introduced as an alternative method for generating circular polarization without relying on tiny polarizer structures and dielectric slabs [11–14]. The ATSA and CWSA described exhibit wideband circular polarization. However, their applicability as reflector feed source has yet to be evaluated.

This paper proposes a novel waveguide antenna design that utilizes Nabla slot (NS) on its aperture to function as a polarizing element, proving the necessary phase transition for the generation of left-hand circular polarization (LHCP). It provides impedance matching ($S_{11} \leq -10$ dB) from 12 to 15.2 GHz and AR ≤ 3 dB from 13. to 15.2 GHz. Moreover, the antenna demonstrates a well-symmetric radiation pattern in the main lobe and nearly identical 12 dB half beamwidth in its principal planes within the frequency range of 13.4–15.2 GHz.

© The Author(s), 2025. Published by Cambridge University Press in association with The European Microwave Association.

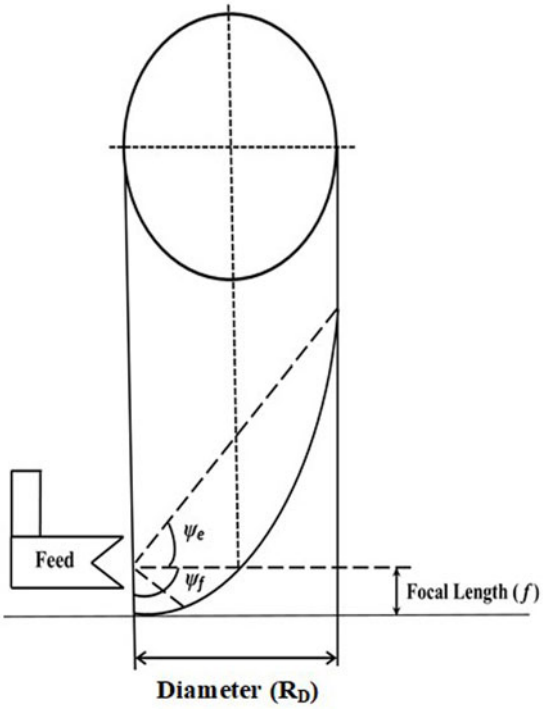



**Figure 1.** Offset parabolic reflector antenna configuration.

## Feed requirement

The proposed waveguide antenna designed to act as a feed for a parabolic reflector being offset with $f/R_D$ ratio of 0.25. The offset reflector antenna configuration mitigates aperture blockage by the primary feed, thereby reducing scattered radiation and improving system gain. Fig. 1 shows the key angles for the offset configuration, $\psi_e$ denotes half cone angle held at the outer edge of the reflector, and $\psi_f$ denotes the angle between the feed and the focal axis. The proposed antenna and the reflector need to fit inside the small satellite volume. For this purpose, $f/R_D$ ratio of 0.25, reflector diameter ($R_D$) of 10 cm, and lower rim offset ($H$) of zero are chosen.

$$\psi_e = tan^{-1}\frac{2fR_D}{4f^2 + H(R_D + H)} = 63.44^\circ \quad (1)$$

$$\psi_f = 2tan^{-1}\frac{2H + R_D}{4f} = 90^\circ \quad (2)$$

Therefore, half cone angle held at the outer edge of the reflector ($\psi_e$) should be 63.44 degrees as given in equation (1). For optimal performance, reflector antennas need controlled edge taper (power difference between center and edge of the reflector). Higher illumination taper (e.g., 15 dB or more) can result in lower sidelobe levels, but it also decrease the efficiency of the antenna. Alternatively, a lower illumination taper (e.g., 9 dB or less) can result in higher antenna efficiency, but it may also lead to higher sidelobe levels. The 12 dB edge taper illumination balances side lobe suppression and antenna efficiency [15]. Therefore, the proposed feed source is designed to have a 12 dB half beamwidth of around 64° within the operating bandwidth. The feed antenna should be positioned at an angle ($\psi_f$) of 90° offset from the focal axis of the offset reflector, as indicated in equation (2) [16], which will make feed arrangement simpler.

## Antenna configuration and operating principle of polarizer

### *Proposed antenna structure*

The 3D profile of the proposed waveguide antenna made of aluminum is shown in Fig. 2. The circular waveguide, excited by a side-coupled rectangular waveguide, creates a T-shaped junction. The proposed feed using this side fed design, thereby eliminating the need for a rectangular-to-circular waveguide transition and reducing the overall antenna length. A 45-degree offset exists between the input port and the NS on the waveguide aperture. The structural details of the proposed antenna are shown in Fig. 3.

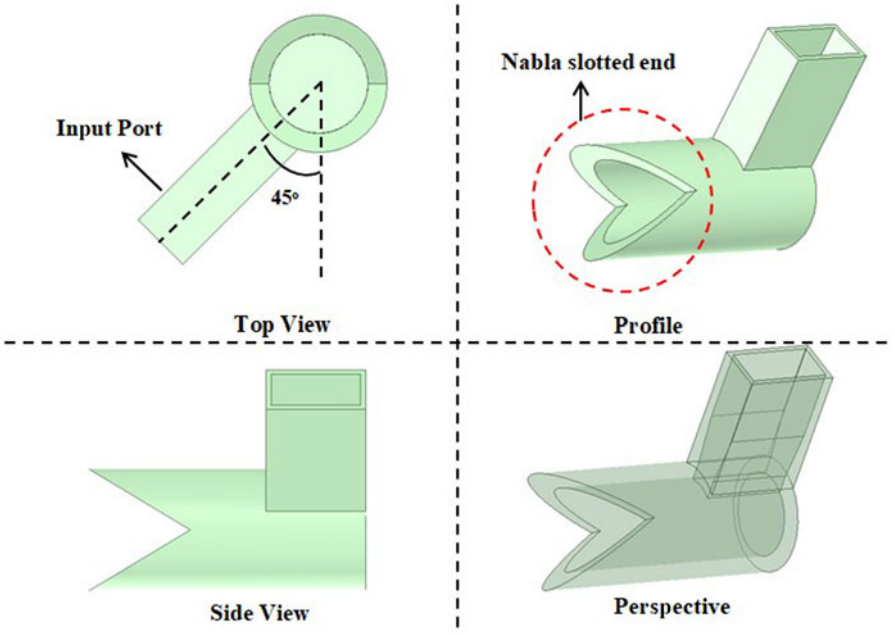



**Figure 2.** Proposed waveguide antenna 3D profile.

https://doi.org/10.1017/S1759078725102742 Published online by Cambridge University Press

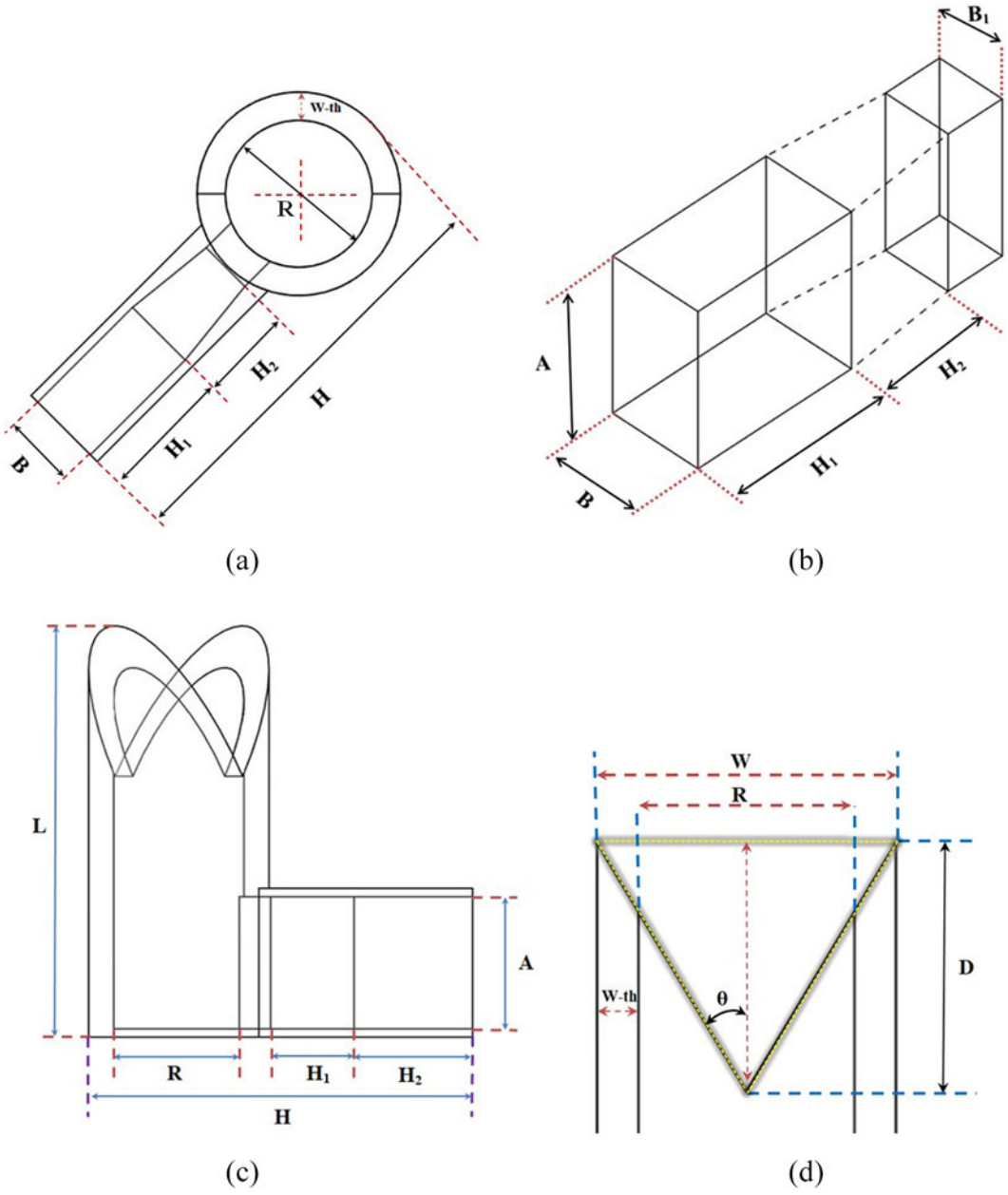



**Figure 3.** Geometry of the proposed waveguide antenna (a) top view (b) tapered portion of the rectangular waveguide (c) side view (d) Nabla slotted section of the proposed waveguide antenna.

A standard WR62 rectangular waveguide, with dimensions A and B denoting its height and width, serves as the input port. To achieve better impedance matching between circular and rectangular waveguides, the input port position was optimized. As in [17], the rectangular waveguide's width was linearly tapered from $B$ to $B_1$ at the input junction, shown by the dashed line in Fig. 3(b). The length of this tapered section, denoted as $H_2$, was also subjected to optimization to enhance impedance matching bandwidth and improve return loss and $H_1$ denotes the length of the standard WR62 waveguide. A significant correlation was observed between the tapered width ($B_1$), tapered length ($H_2$), and the reflection coefficient ($S_{11}$) of the input port. Specifically, an increment in $H_2$ resulted in a corresponding decrease in the reflection coefficient, indicating improved conversion efficiency from the $TE_{10}$ mode in the rectangular waveguide to the $TE_{11}$ mode in the circular waveguide. The diameter ($R$) of the circular waveguide is 0.73 $\lambda$, where $\lambda$ denotes the wavelength of the center frequency 14 GHz, respectively. The overall length ($L$) and breadth ($H$) of the proposed antenna is represented as $L$ and $H$. $W$th denotes the thickness of the circular waveguide. Width ($W$) of the NS is similar to the circular waveguide's outer diameter and it forms inverted symmetric half cone angle ($\theta$) and $D$ denotes slot depth. The proposed antenna has a simple structure.

### *Principle of CP generation*

The following discussion explains the principle of operation. A rectangular LP $TE_{10}$ mode, excited at the chosen input port, is

https://doi.org/10.1017/S1759078725102742 Published online by Cambridge University Press

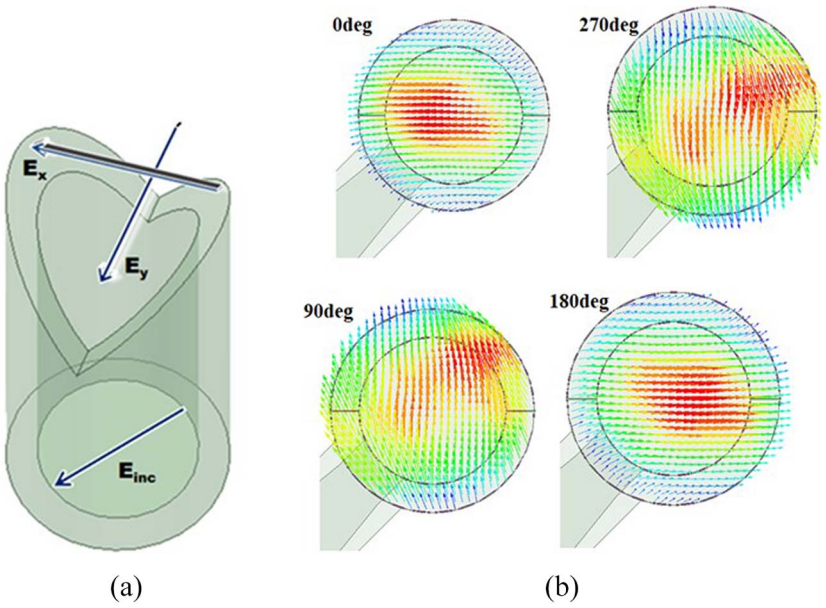



**Figure 4.** (a) Output field components in the Nabla slot (NS) section of waveguide antenna. (b) Effect of NS on the *E* fields in the aperture of the waveguide antenna leading to LHCP.

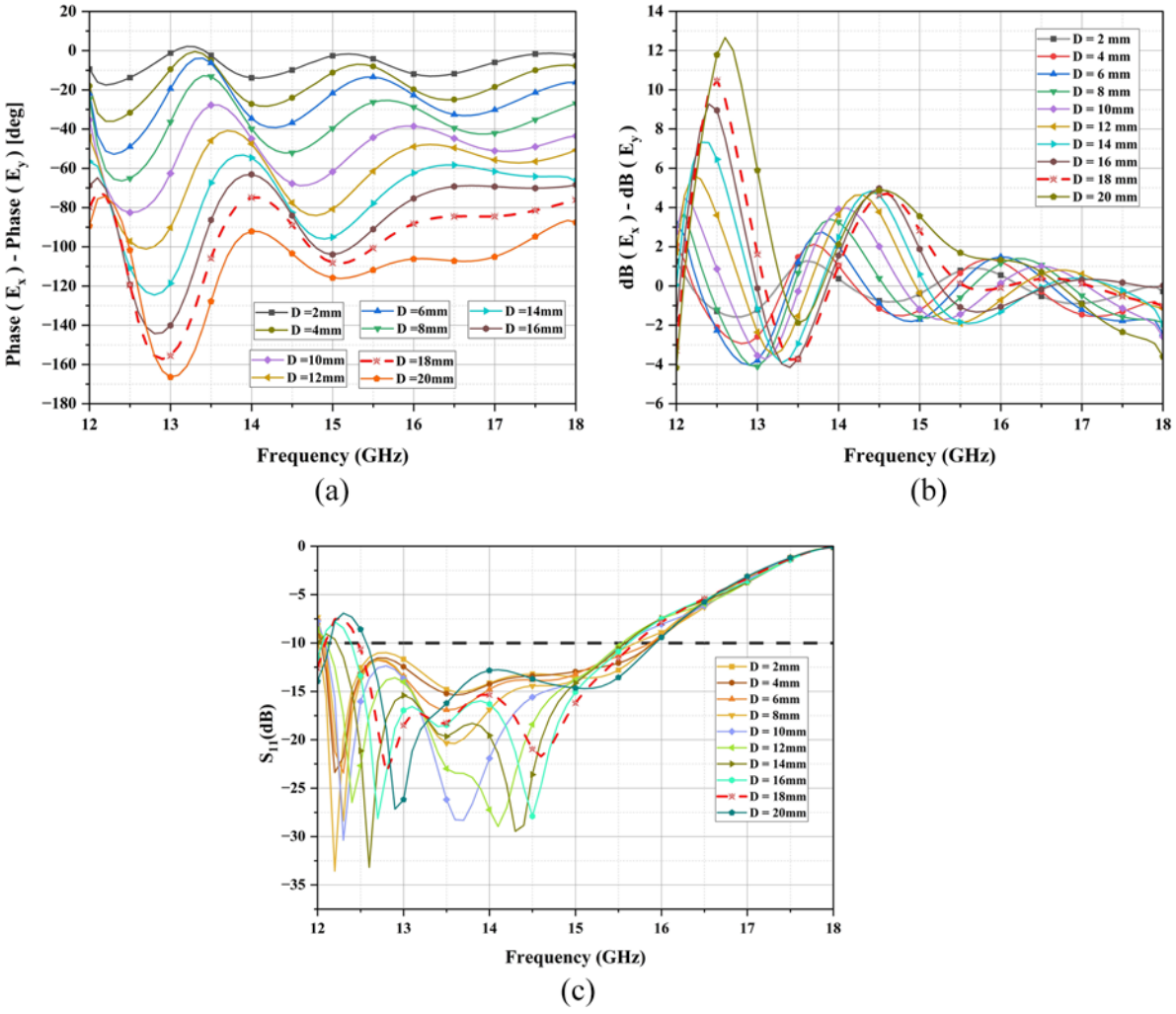



**Figure 5.** Simulated orthogonal far field (a) phase difference (b) amplitude difference and (c) $S_{11}$ plot under different values of $D$ when $W = 8.8$ mm and $L = 2\ \lambda$.

https://doi.org/10.1017/S1759078725102742 Published online by Cambridge University Press

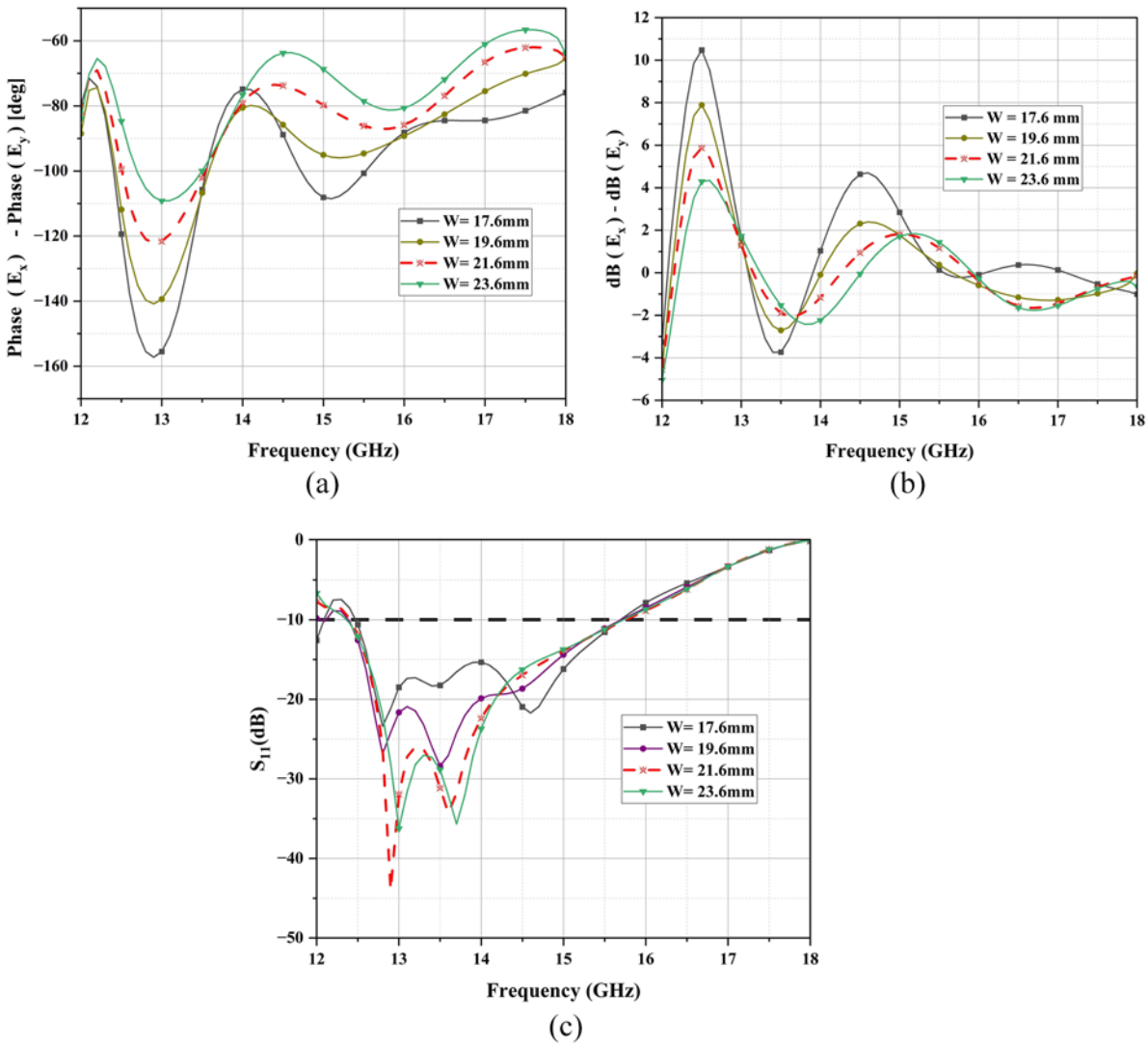



**Figure 6.** Simulated orthogonal far field (a) phase difference (b) amplitude difference and (c) $S_{11}$ plot under different values of $W$ when $D = 18$ mm and $L = 2\lambda$.

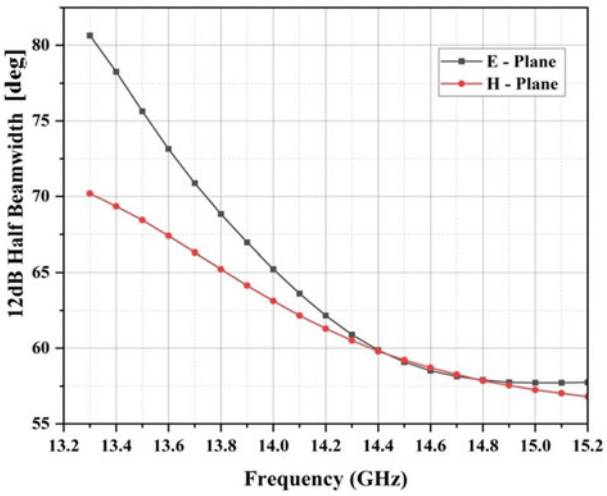



**Figure 7.** Simulated 12 dB half beamwidth of $E$ plane and $H$ plane for $D = 18$ mm, $W = 21.6$ mm, and $L = 2\lambda$.

https://doi.org/10.1017/S1759078725102742 Published online by Cambridge University Press

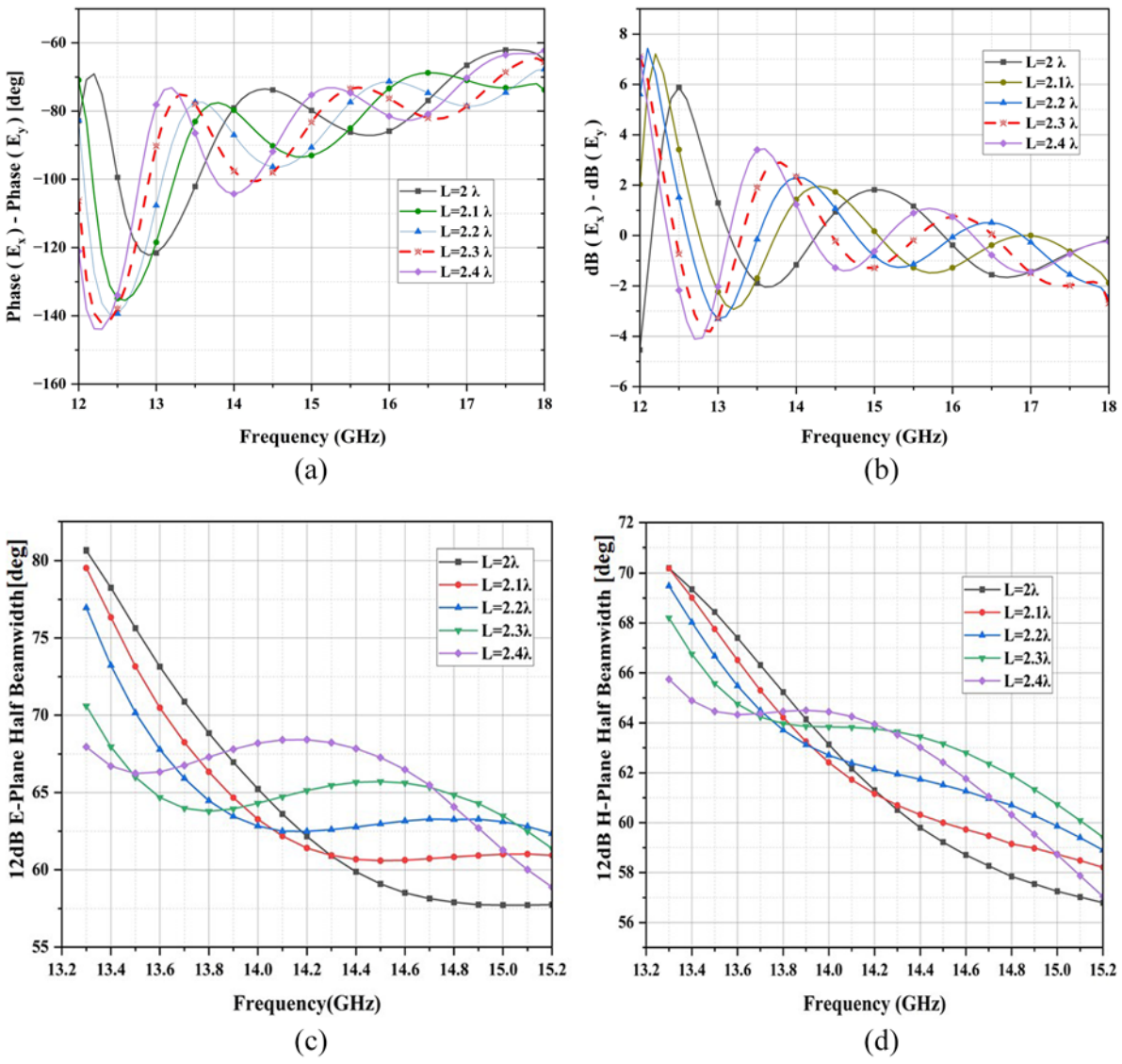



**Figure 8.** Simulated (a) orthogonal far field phase difference (b) amplitude difference (c) 12 dB half beamwidth of *E* plane and (d) *H* plane under different values of *L* when $D = 18$ mm and $W = 21.6$ mm.

converted to an LP $TE_{11}$ mode within the circular waveguide. The resulting $TE_{11}$ mode, characterized by its electric fields perpendicular to the direction of propagation offer distinct advantages for generating dual or circularly polarized radiation due to its low loss and efficient propagation [18]. Subsequently, a 45-degree offset between the input port and the NS on the aperture induces the decomposition of the incident E-field ($\overrightarrow{E_{inc}}$) of $TE_{11}$ mode into two orthogonal components, and $\overrightarrow{E_y}$ which can be written as

$$\overrightarrow{E_{inc}} = \overrightarrow{E_x} + \overrightarrow{E_y} \tag{3}$$

$$\overrightarrow{E_x} = a_x \left|\overrightarrow{E_x}\right| \cos(wt + \phi_x) \tag{4}$$

$$\overrightarrow{E_y} = a_y \left|\overrightarrow{E_y}\right| \cos(wt + \phi_y), \tag{5}$$

where $a_x$ and $a_y$ denote the unit vectors, while $\phi_x$ and $\phi_y$ indicate the phases of the electric field components $\overrightarrow{E_x}$ and $\overrightarrow{E_y}$, respectively. The condition for generating LHCP is that the two orthogonal components must have identical magnitudes and a 90-degree phase shift between them. That is

$$\left|\overrightarrow{E_x}\right| = \left|\overrightarrow{E_y}\right|, \tag{6}$$

$$\left|\overrightarrow{E_x}\right| - \left|\overrightarrow{E_y}\right| = 0, \tag{7}$$

$$\phi_x - \phi_y = -90^0. \tag{8}$$

By adjusting the slot dimensions ($D$ and $W$) and the length of the circular waveguide ($L$), a minimum amplitude variation and −90° phase difference between the far-field components ($\overrightarrow{E_x}$ and $\overrightarrow{E_y}$) can be achieved to generate LHCP. As depicted in Fig. 4(a), $\overrightarrow{E_y}$ aligns with the slot's cut direction, while $\overrightarrow{E_x}$ is parallel to the NS. The circular waveguide's radius influences the propagation constants of $\overrightarrow{E_y}$ and $\overrightarrow{E_x}$. The NS introduces a differential propagation constant, resulting in $\overrightarrow{E_y}$, aligned with the cut, experiencing a λ/4 phase delay relative to the orthogonal field at the aperture. The effect of NS

https://doi.org/10.1017/S1759078725102742 Published online by Cambridge University Press

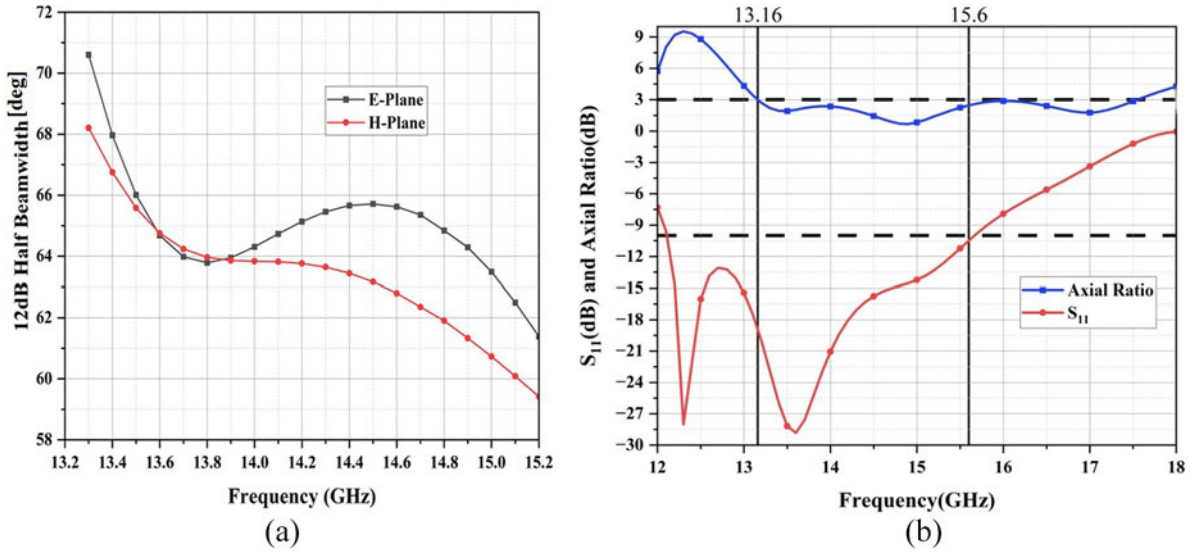



**Figure 9.** Simulated (a) 12 dB half beamwidth of *E* plane and *H* plane (b) $S_{11}$ and AR plot for the optimized parameters, as shown in Table 1.

**Table 1.** Optimized parameters of the proposed antenna design

| *L*/mm | *H*/mm | *A*/mm | *B*/mm | $H_1$/mm | $H_2$ /mm |
|---|---|---|---|---|---|
| 49.2 | 46 | 15.86 | 7.899 | 14.2 | 10 |
| **$B_1$/mm** | ***W*th** | ***W*/mm** | ***R*/mm** | ***D*/mm** | **θ/degree** |
| 5.8 | 3 | 21.6 | 15.6 | 18 | 23.4 |

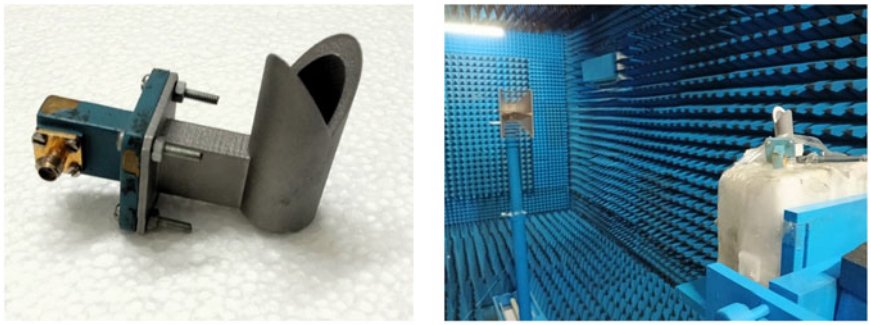



**Figure 10.** Photograph of (a) the fabricated proposed waveguide antenna, with a WR62 waveguide-to-coax adapter at the input. (b) Measurement set-up for the waveguide antenna prototype in an anechoic chamber.

on the *E* field in the proposed antenna aperture is analyzed using Ansys HFSS. The LHCP wave is generated using the NS, as shown in Fig. 4(b). The detailed parametric study on slot dimensions (*D* and *W*) and circular waveguide length (*L*) has been conducted to analysis the influence of these parameters on the phase and amplitude difference of $\overrightarrow{E_x}$ and $\overrightarrow{E_y}$ components and 12 dB half beamwidth (*E* and *H* plane). From the simulation result, it is observed that the key advantage of the NS is its gradual perturbation in the circular waveguide aperture which facilitates circular polarization with balanced 12 dB half-beamwidth in both *E* and *H* planes across the desired frequency band.

## Parametric studies

A parametric study was undertaken to assess the sensitivity of the system to variations in NS dimensions (*W, D*) and circular waveguide length (*L*). The goal is to optimize these parameters to minimize amplitude variations and achieve phase difference of –90° between $\overrightarrow{E_x}$ and $\overrightarrow{E_y}$ in the far field, thereby generating a LHCP with an axial ratio below 3 dB within the Ku band. Furthermore, the design targets to produce identical 12 dB half beamwidth in the principal planes. A lower axial ratio signifies better circular polarization quality. For most circular polarization applications, including satellite communications and radar systems, an axial ratio below 3 dB is typically acceptable. Additionally, nearly equal 12 dB half beamwidth with a symmetric radiation pattern in principal planes are essential for reflector antenna applications. Initially, the circular waveguide length ($L = 2\lambda$) and its outer diameter ($W = 17.6$ mm) were maintained constant.

### *Varying the slot depth (D)*

Figure 5 illustrates the impact of varying depth (D) on the phase and amplitude differences between the orthogonal far-field

https://doi.org/10.1017/S1759078725102742 Published online by Cambridge University Press

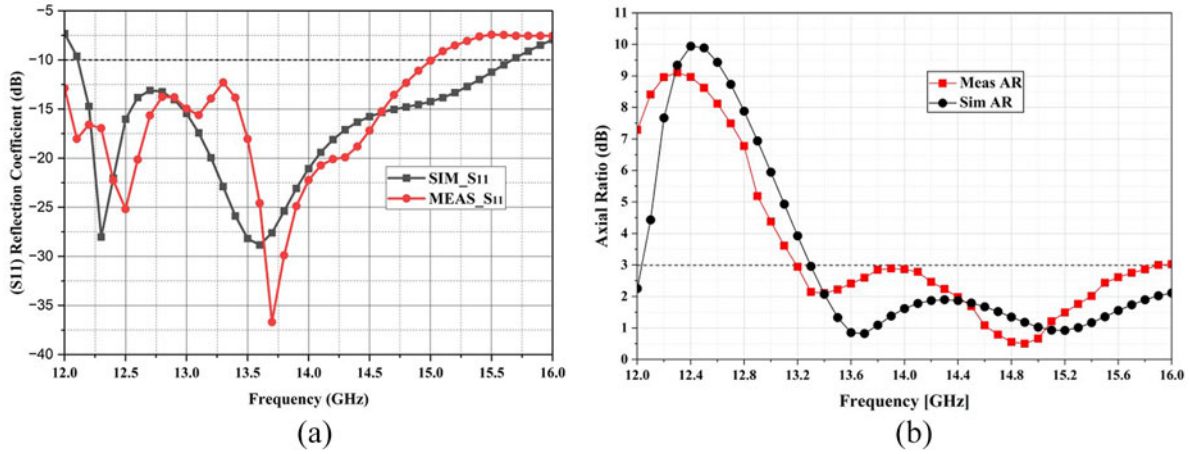



**Figure 11.** Simulated and measured (a) reflection coefficient and (b) axial ratio of the proposed waveguide antenna feed as a function of frequency.

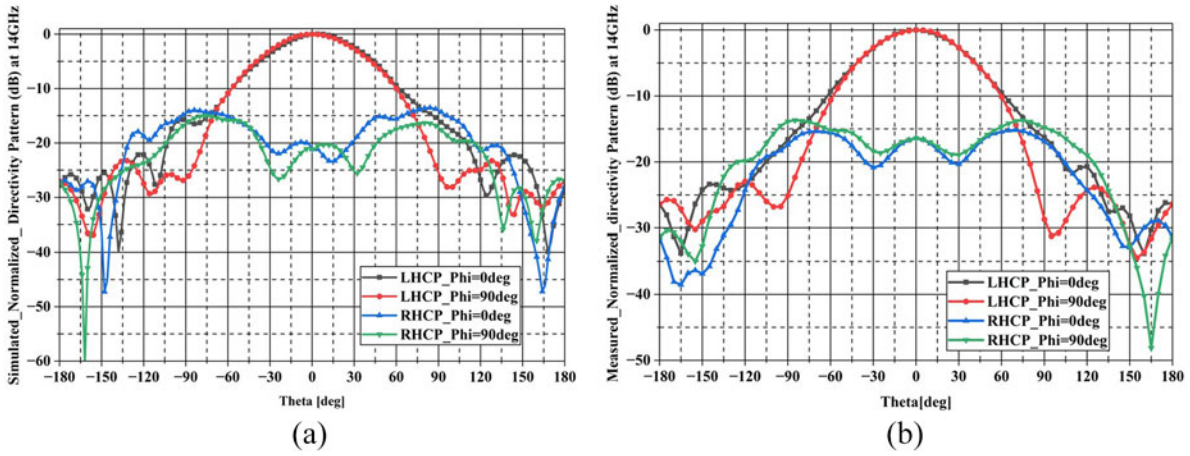



**Figure 12.** (a) Simulated and (b) measured normalized directivity patterns of the proposed waveguide antenna at 14 GHz for both polarizations.

components $\overrightarrow{E_x}$ and $\overrightarrow{E_y}$ at bore sight and $S_{11}$ of the proposed antenna. Increasing the NS depth (D) from 2 to 18 mm yielded a positive impact on phase difference for frequencies exceeding 13.5 GHz but the lower frequencies exhibiting a maximum phase difference of −160°. Conversely, this depth increment resulted in a significant amplitude imbalance below 13 GHz, reaching a peak of 10.7 dB at 12.5 GHz for $D = 18$ mm, accompanied by a deterioration in impedance bandwidth and return loss. Further augmentation of $D$ beyond 18 mm led to an undesirable phase difference across the entire frequency band and a pronounced amplitude imbalance exceeding 10.7 dB, further compromising impedance bandwidth and return loss. Therefore, an NS depth (D) of 18 mm was determined as the optimal value.

### *Varying the slot width (W)*

It has been established that the wall thickness and length of a circular waveguide influences its radiation characteristics [19, 20]. In this context, increasing the outer diameter of the circular waveguide, which in turn leads to an increment in the slot width ($W$), has been found to have a positive impact on the phase and amplitude difference of orthogonal components at bore sight and reflection coefficient which is shown in Fig. 6. Increasing the width ($W$) from 17.6 to 23.6 mm (i.e. increasing the circular waveguide's thickness ($W$th) from 1 to 4 mm) while maintaining a constant depth ($D$) of 18 mm. It has been observed that the phase and amplitude differences of the far-field components at $W = 23.6$ mm are more favorable for generating LHCP compared to the previously mentioned conditions (5) and (6). However, as noted in reference [19], increasing the thickness also results in higher cross-polarization for the proposed feed. To maintain the thickness at an optimal level, $W = 21.6$ mm has been selected as the ideal value, as it provides improved phase difference, amplitude difference, and return loss characteristics.

It is necessary to verify whether the desired equal 12 dB half beamwidth is attained in the principal planes. 12 dB half beamwidth for $D = 18$ mm, $W = 21.6$ mm, and circular waveguide length of $2\lambda$ is shown in the Fig. 7, which indicates that there is a considerable variation in the 12 dB half beamwidth on the principle planes and it is not around 64°.

### *Varying the circular waveguide length (L)*

To optimize the 12 dB half-beamwidth and enhance the stability of amplitude and phase differences within the frequency range where $S_{11} \leq -10$ dB, the length of the circular waveguide was gradually increased from $2\lambda$ to $2.4\lambda$. The resulting effects are illustrated in Fig. 8. It is observed that when the circular waveguide length

https://doi.org/10.1017/S1759078725102742 Published online by Cambridge University Press

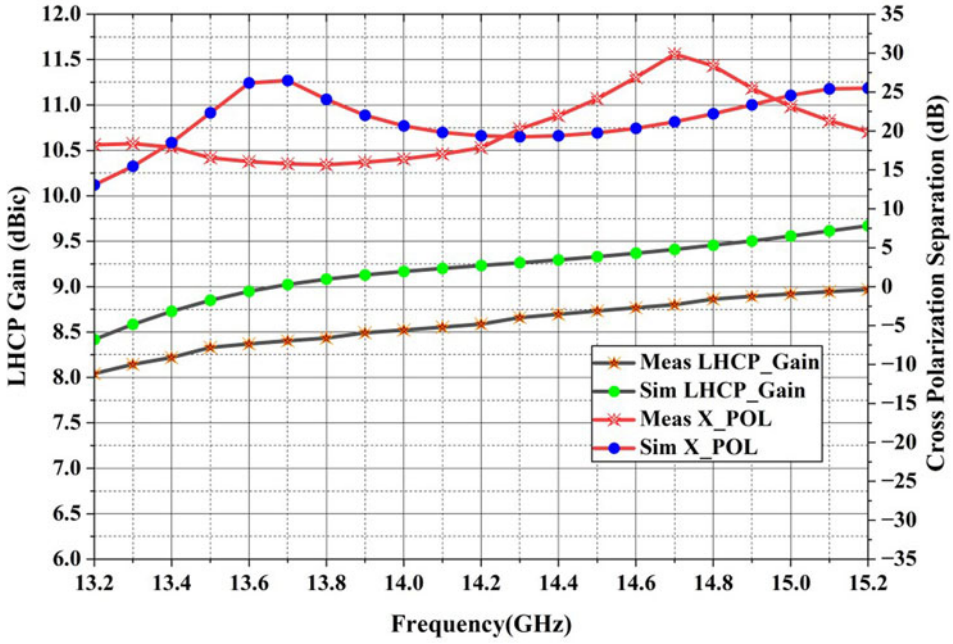



**Figure 13.** Comparison of simulated and measured LHCP gain and cross-polarization separation of the proposed feed as a function of frequency.

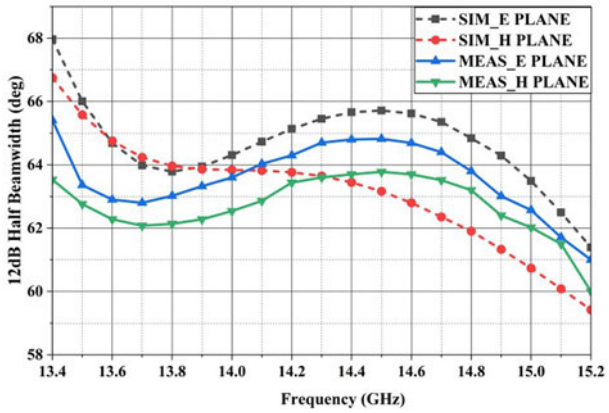



**Figure 14.** Comparison of simulated and measured 12 dB half beamwidth of the proposed feed as a function of frequency.

**Table 2.** Measured Performance characteristics of the proposed waveguide antenna design

| Proposed antenna | Impedance matching bandwidth ($S_{11} \leq -10$ dB) | Circular polarization bandwidth (AR ≤ 3 dB) | Pattern bandwidth (equal 12 dB half beamwidth in *E* and *H* plane) | LHCP Gain (dBic) | Max cross-polarization separation level |
|---|---|---|---|---|---|
| | 12–15.2 GHz (23.5%) | 13.2–15.2 GHz (14%) | 13.4–15.2 GHz (12.5%) | 8.2–8.9 (±0.5) | 29 dB at 14.7 GHz |

of 2.3$\lambda$ achieves a −90°(±15°) phase difference and low amplitude variation (maximum 3 dB) from 13.16 to 17.55 GHz, generating LHCP in this range. This also results in nearly equal 12 dB half-beamwidth of around 65° in the *E* and *H* planes from 13.4 to 15.1 GHz. Figure 9(a) and (b) illustrates the $S_{11}$ plot, axial ratio plot, and 12 dB half-beamwidth of the proposed waveguide antenna. The achieved axial ratio bandwidth, which aligns with the impedance bandwidth ($S_{11}$ below −10 dB from 12.11 to 15.6 GHz), ranges from 13.16 to 15.6 GHz, representing a 16.9% bandwidth. Additionally, the pattern bandwidth (12 dB half-beamwidth around 65°) that matches both the impedance and axial ratio bandwidth spans from 13.4 to 15.2 GHz, covering a 12.5% bandwidth. These simulation results satisfy the requirements for illuminating the offset parabolic reflector with the desired $f/R_D$ ratio. Table 1 provides the optimized parameters of the proposed waveguide antenna.

## Design procedure

***Requirement***: Axial ratio ≤3 dB, $S_{11} \leq -10$ dB, equal 12 dB half beamwidth around 64deg (*E* and *H* plane) within the Ku-band frequency range:

https://doi.org/10.1017/S1759078725102742 Published online by Cambridge University Press

**Table 3.** Comparison of proposed LHCP waveguide antenna to the other CP antennas

| REF | Impedance bandwidth | 3 dB AR bandwidth | Gain (dBic) | Method to generate CP | Volume ($\lambda_0 \times \lambda_0 \times \lambda_0$) |
|---|---|---|---|---|---|
| [22] (2016) | 3.5% (14–14.5 GHz) | 9%(13.6–14.9 GHz) | 8.07 | Required extra circuit to produce CP | 0.74 × 0.82 × 1.44 |
| [23] (2017) | 5% (23.7–24.9 GHz) | 5% (23.7–24.9 GHz) | 8.5 | Phase controlling and power dividing structure | 7.59 × 4.07 × 0.12 |
| [24] (2018) | 9.5% (28–30.8 GHz) | 7.4% (28.5–30.8 GHz) | 13–14.2 | Thin Polarizer | 3.00 × 1.76 × 1.41 |
| [25] (2019) | ~20.7% (6.95–8.68 GHz) | ~9.6% (7.47 – 8.25 GHz) | ~5 | H-shaped conformal metal strip | 0.57 × 0.457 × 0.30 |
| [26] (2021) | 3.4% (28.99–30 GHz) | 1% (29.35–29.64 GHz) | For single element peak gain is 6.78 | T-shaped slot | 1.09 × 1.29 × 0.44 |
| [27] (2025) | 7.4% (9.63–10.37 GHz) | 7% (9.65–10.35 GHz) | 7.5 | L-shaped slot | 1.20 × 0.89 × 0.47 |
| **This Work** | **23.5% (12–15.2 GHz)** | **14% (13.2–15.2 GHz)** | **8.2–8.9** | **Nabla slot (NS)** | **2.29 x 1.01 x 2.15** |

- Design a conventional circular waveguide with a diameter ($R$) of 0.73λ, a length ($L$) of 2λ, and a wall thickness ($W$th) of 1 mm.
- For Ku-band operation, a standard WR62 rectangular waveguide is selected as the input port, with dimensions $A = 15.79$ mm and $B = 7.8$ mm.
- Construct a $T$-junction by joining the circular and rectangular waveguides. Perform iterative adjustments of the input port position to minimize impedance mismatch.
- To improve impedance matching bandwidth and return loss, based on [17], the breadth ($B$) of the WR62 waveguide is linearly tapered to an optimal range, over a length of $H_2$ at the input junction.
- Cut a Nabla ($\nabla$) shaped slot on the circular waveguide aperture with a slot width ($W = R + 2 * W$th) and an initial depth ($D = 2$ mm). The slot should be positioned with a 45-degree offset relative to the input port to generate CP.
- Iteratively optimize the slot width ($W$), depth ($D$), and cylindrical waveguide length ($L$) until the desired performance requirements are met.
- The proposed design can be modified to operate at any target frequency range to achieve the above-mentioned requirements.

## Measured results of proposed waveguide antenna

Figure 10(a) depicts the photograph of the 3D-printed waveguide antenna, and Fig. 10(b) shows the experimental measurement setup. The proposed waveguide antenna was fabricated from aluminum using the Direct Metal Laser Sintering (DMLS) additive manufacturing process. The waveguide antenna parameters were measured using a Keysight N9917A Vector Network Analyzer (VNA). An LP horn antenna served as the transmitting antenna, and the measurement procedure followed the methodology outlined in [21]. Figure 11 shows the comparison of simulated and measured reflection coefficient and axial ratio as a function of frequency. The measured $S_{11}$ value below −10 dB from the range of 12–15.2 GHz, corresponding to the impedance matching bandwidth of 23.5%. The slight variation observed between the simulated and measured impedance matching bandwidths may be attributed to fabrication tolerances. The axial ratio (AR) of the feed waveguide antenna was measured to be ≤3 dB from the range of 13.2–16 GHz, indicating strong agreement with the corresponding simulation data. The measured AR bandwidth range 13.2–15.2 GHz aligns with matches the measured impedance bandwidth ($S_{11} \leq -10$ dB from 12 to 15.2 GHz) and represents a 14% AR bandwidth. Figure 12 presents the simulated and measured normalized directivity pattern of co-polarized (LHCP) and cross-polarized field (RHCP) at 14 GHz. The results show the excellent correlation in terms of beamwidth and symmetrical pattern. Figure 13 compares the simulated and measured LHCP gain and cross-polarization separation of the proposed feed. The simulated LHCP gains are 8.42, 9.23, and 9.6 dBic, and the cross-polarization separation (co-polarization LHCP – cross-polarization RHCP) are 13.06, 19, and 25.4 dB at 13.2, 14.2, and 15.2 GHz, respectively. The measured LHCP gain of the proposed feed are 8.04, 8.55, and 8.9 dBic, and the cross-polarization separation are 18.21, 17.85, and 19.89 dB at 13.2, 14.2, and 15.2 GHz, respectively, and maximum cross-polarization separation is 29.8 dB at 14.7 GHz. The variations in the measured and simulated results are likely due to the fabrication and measurement tolerances. Figure 14 compares the simulated and measured 12 dB half beamwidth of the proposed waveguide antenna. Over the 13.4–15.2 GHz range, which aligns with AR bandwidth, the antenna exhibits an average measured 12 dB half beamwidth of approximately 65°. This performance satisfies the illumination requirements for an offset parabolic reflector with an $f/R_D$ ratio of 0.25. Table 2 presents the measured performance characteristics of the waveguide antenna. Table 3 compares the proposed antenna performance with other circularly polarized antennas.

## Pros and cons of the proposed design

*Pros*:

- Compact and low profile.
- Cost efficient and simple structure.
- Better cross-polarization separation (≤19 dB).
- Lower Side lobe level (≥ −20 dB).

https://doi.org/10.1017/S1759078725102742 Published online by Cambridge University Press

- Suitable to act as a feed source in an offset parabolic reflector with an $f/R_D$ ratio of 0.25.

*Cons*:

- The proposed Ku-band waveguide antenna is primarily suited for 12 U CubeSat applications. It is not appropriate for integration into satellite smaller than the CubeSat standard.

## Conclusion and future work

By combining the properties of NS and circular waveguide, low profile and compact LHCP waveguide antenna operating in Ku band is designed which will eliminates the dependence on complex internal structures within the waveguide cavity to generate CP. The analysis and simulation results were validated through the fabrication and measurement of the proposed feed waveguide antenna. The proposed feed antenna has $S_{11} \leq -10$ dB from 12–15.2 GHz, AR (below 3 dB) performance from 13.2 to 15.2 GHz, good symmetric radiation pattern in main lobe and exhibits 12 dB half edge illumination of around 65° in its principal planes from 13.4 to 15.2 GHz. Thereby meeting the requirements for illuminating the offset parabolic reflector with a 0.25 $f/R_D$ ratio, as mentioned in Section II.

**Data availability statement.** The authors have nothing to report.

**Acknowledgements.** The financial support from The Institution of Engineers (India) for the antenna measurements in this subject is gratefully acknowledged [grant no: DR2025013]. The authors thank the Mepco Agilent R&D Centre, as well as the management and principal of Mepco Schlenk Engineering College, for their support and resources.

**Competing interests.** The authors declare no conflicts of interest.

## References

1. **Steven Shichang Gao, Qi Luo and Fuguo Zhu** (2014) Introduction to circularly polarized antennas In *Circularly Polarized Antennas*. Chichester, UK: Wiley, pp. 1–25.
2. **Illahi U, Iqbal J, Ramay SM and Sulaiman MI** (2024) Design and development of a new circularly polarized MIMO wearable DRA for WBAN applications. *AEU - International Journal of Electronics and Communications* **177**, 155208. https://doi.org/10.1016/j.aeue.2024.155208
3. **Shafai L, Sharma SK and Rao S** (2013) *Handbook of Reflector Antennas and Feed Systems: Feed Systems*. Vol. **II**. Norwood, MA: USA: Artech House.
4. **Sharma SK, Shafai L and Rao S** (2013) *Handbook of Reflector Antennas and Feed Systems: Theory and Design of Reflectors*. Vol. I. Norwood, MA, USA: Artech House.
5. **Virone G, Tascone R, Peverini OA and Orta R** (2007) Optimum-iris-set concept for waveguide polarizers. *IEEE Microwave and Wireless Components Letters* **17**(3), 202–204. https://doi.org/10.1109/LMWC.2006.890474
6. **Agnihotri I and Sharma SK** (2019) Design of a compact 3-D metal printed Ka-band waveguide polarizer. *IEEE Antennas and Wireless Propagation Letters* **18**(12), 2726–2730. https://doi.org/10.1109/LAWP.2019.2950312
7. **Luo N, Yu X, Mishra G and Sharma SK** (2020) A millimeter-wave (V-Band) dual-circular-polarized horn antenna based on an inbuilt monogroove polarizer. *IEEE Antennas and Wireless Propagation Letters* **19**(11), 1933–1937. https://doi.org/10.1109/LAWP.2020.3015745
8. **Bornemann J, Amari S, Uher J and Vahldieck R** (1999) Analysis and design of circular ridged waveguide components. *IEEE Transactions on Microwave Theory & Techniques* **47**(3), 330–335. https://doi.org/10.1109/22.750235
9. **Song M, Zhang X, Wang Z, Xu D, Loh TH and Gao S** (2024) 3-D-printed spiral inverted ridge circularly polarized horn antenna with one octave bandwidth. *IEEE Antennas and Wireless Propagation Letters* **23**(10), 3018–3022. https://doi.org/10.1109/LAWP.2024.3418498
10. **Wang S-W, Chien C-H, Wang C-L and Ruey-Beei W** (2004) A circular polarizer designed with a dielectric septum loading. *IEEE Transactions on Microwave Theory & Techniques* **52**(7), 1719–1723. https://doi.org/10.1109/TMTT.2004.830487
11. **Yao Y, Cheng X, Yu J and Chen X** (2016) Analysis and design of a novel circularly polarized antipodal linearly tapered slot antenna. *IEEE Transactions on Antennas and Propagation* **64**(10), 41784187. https://doi.org/10.1109/TAP.2016.2593870
12. **Cheng X, Yao Y, Yu T, Chen Z, Yu J and Chen X** (2018) Analysis and design of a low-cost circularly polarized horn antenna. *IEEE Transactions on Antennas and Propagation* **66**(12), 73637367. https://doi.org/10.1109/TAP.2018.2867024
13. **Liu J, Lu H, Li Z, Liu Z, Dong Z, Deng C, Lv X and Liu Y** (2019) Wideband circularly polarized waveguide-fed antipodal exponential tapered slot antenna. *IEEE Antennas and Wireless Propagation Letters* **18**(9), 1912–1916. https://doi.org/10.1109/LAWP.2019.2933539
14. **Yu H-Y, Yu J, Yao Y, Liu X and Chen X** (2020) Wideband circularly polarized horn antenna exploiting open slotted end structure. *IEEE Antennas and Wireless Propagation Letters* **19**(2), 267–271. https://doi.org/10.1109/LAWP.2020.2964623
15. **Amyotte E, Gimersky M and Donato M** (2001) High performance Ka-band multibeam antennas, 19th International Communications Satellite Systems Conference, Toulouse, France, April, Section 31, p. 964.
16. **Milligan TA** (2005) *"Reflector Antennas," in Modern Antenna Design*. Hoboken, NJ, USA: Wiley, p. 580.
17. **Johnson RC** (1959) Design of linear double tapers in rectangular waveguides. *IRE Transactions on Microwave Theory and Techniques* **7**(3), 374–378. https://doi.org/10.1109/TMTT.1959.1124594
18. **A.W. Rudge, K. Milne, A.D. Olver and P. Knight**, ed. (1982) *The Handbook of Antenna Design*, vols. **1–2**. London: Peter Peregrinus.
19. **James GL and Greene KJ** (1978) Effect of wall thickness on radiation from circular waveguides. *Electronics Letters* **14**(4), 90–91. https://doi.org/10.1049/el:19780061
20. **Hansen JE and Shafai L** (1977) Cross polarized radiation from waveguides and narrow-angle horns. *Electronics Letters* **13**(11), 313–315. https://doi.org/10.1049/el:19770229
21. **Toh BY, Cahill R and Fusco VF** (2003) Understanding and measuring circular polarization. *IEEE Transactions on Education* **46**(3), 313–318. https://doi.org/10.1109/TE.2003.813519
22. **Gatti RV and Rossi R** (2016) A dual-polarization slotted waveguide array antenna with polarization-tracking capability and reduced sidelobe level. *IEEE Transactions on Antennas and Propagation* **64**(4), 1567–1572. https://doi.org/10.1109/TAP.2016.2526645
23. **Yin Y, Zarghooni B and Wu K** (2017) Single-layered circularly polarized substrate-integrated waveguide horn antenna array. *IEEE Transactions on Antennas and Propagation* **65**(11), 6161–6166. https://doi.org/10.1109/TAP.2017.2754472
24. **Lin C, Ge Y, Bird TS and Liu K** (2018) Circularly polarized horns based on standard horns and a metasurface polarizer. *IEEE Antennas Wireless Propag Lett* **17**(3), 480–484.
25. **Illahi U, Iqbal J, Sulaiman MI, Alam MM, Su'Ud MM, Jamaluddin MH and Yasin MNM** (2019) Design of new circularly polarized wearable dielectric resonator antenna for off-body communication in WBAN applications. *IEEE Access* **7**, 150573–150582. https://doi.org/10.1109/ACCESS.2019.2947772
26. **Dimitrov KC, Lee Y, Min B-W, Park J, Jeong J and Kim H-J** (2020) Circularly polarized T-shaped slot waveguide array antenna for satellite communications. *IEEE Antennas and Wireless Propagation Letters* **19**(2), 317–321. https://doi.org/10.1109/LAWP.2019.2961386

27. **Rashad H. Mahmud, Mustafa M. Mohammed, Halgurd N. Awl, Yadgar I. Abdulkarim, Ramin Khosravi, Idris H. Salih and Majeed Hasan Mahmood** (2025) A 3D-printed circularly polarized cavity-based slotted waveguide antenna for kidney cancer detection application. *Results in Engineering* **26**, 105458. https://doi.org/10.1016/j.rineng.2025.105458



**Mr. R. R. Sorna Kumar** received the BE degree in Electronics and Communication Engineering from Hindustan College of Engineering and Technology, Coimbatore, Tamil Nadu, India, in 2019, and ME degree in Communication Systems in Mepco Schlenk Engineering College, Sivakasi, Tamil Nadu, India, in 2022. He is currently pursuing PhD at the Department of Electronics and Communication Engineering, Mepco Schlenk Engineering College, India, in Antenna Design. **E-mail**: sornakumarrr@mepcoeng.ac.in



**Dr. Indumathi Ganesan** has 27 years of experience in teaching and research at Mepco Schlenk Engineering College, India. She obtained her Doctoral program in the field of Wireless Communication from Anna University, Chennai, India. Currently, she is working as a Senior Professor in the Department of Electronics and Communication Engineering in Mepco Schlenk Engineering College, Sivakasi, Tamil Nadu, India. She is a lifetime member of ISTE, IEI, and FIETE. Her main research interests are wireless communication, digital signal processing, and antenna design. **E-mail**: gindhu@mepcoeng.ac.in

https://doi.org/10.1017/S1759078725102742 Published online by Cambridge University Press